Airborne Earth Observation Positioning and Orientation by SINS/GPS Integration Using CD R-T-S Smoothing

Xiaolin Gong and Tingting Qin

(*Science and Technology on Inertial Laboratory, Key Laboratory of Fundamental Science for National Defense-Novel Inertial Instrument and Navigation System Technology and BeiHang University, School of Instrumentation Science and Opto-electronics Engineering; all Beijing, China*)
(E-mail: gongxiaolin@buaa.edu.cn)

This paper addresses the issue of state estimation in the integration of a Strapdown Inertial Navigation System (SINS) and Global Positioning System (GPS), which is used for airborne earth observation positioning and orientation. For a nonlinear system, especially with large initial attitude errors, the performance of linear estimation approaches will degrade. In this paper a nonlinear error model based on angle errors is built, and a nonlinear estimation algorithm called the Central Difference Rauch-Tung-Striebel (R-T-S) Smoother (CDRTSS) is utilized in SINS/GPS integration post-processing. In this algorithm, the measurements are first processed by the forward Central Difference Kalman filter (CDKF) and then a separate backward smoothing pass is used to obtain the improved solution. The performance of this algorithm is compared with a similar smoother based on an extended Kalman filter known as ERTSS through Monte Carlo simulations and flight tests with a loaded SINS/GPS integrated system. Furthermore, a digital camera was used to verify the precision of practical applications in a check field with numerous reference points. All these validity checks demonstrate that CDRTSS is a better method and the work of this paper will offer a new approach for SINS/GPS integration for Synthetic Aperture Radar (SAR) and other airborne earth observation tasks.

1. INTRODUCTION.   An integrated system comprising a Strapdown Inertial Navigation System (SINS) and Global Positioning System (GPS) has become the main method to derive aircraft trajectory information for airborne earth observation (Groves, 2008). Most observation loads, such as Synthetic Aperture Radar (SAR) and Light Detection and Ranging (LiDAR) depend on a SINS/GPS integrated system for

motion compensation. Furthermore, the imaging quality is affected directly by the motion measurement precision of the SINS/GPS integrated system. For example, low-frequency motion errors (biases and ramps) cause errors in the location of the imagery relative to the Earth or "target location" errors, while higher frequency errors cause images to defocus, even if autofocus algorithms are applied (Kim, 2004). This means that the SINS/GPS integrated system must have high absolute precision as well as relative precision (smoothness) in motion measurement.

In general, a SINS/GPS integrated system used for airborne earth observation comprises an inertial measurement unit (IMU), a GPS receiver, a processing computer system (PCS) and post-processing software (PPS) (Fang and Gong, 2010). The estimation algorithms run in the PCS and PPS, which integrate the SINS and GPS, are the key to the performance of the integrated system. Three classes of optimal estimation algorithms can be found in the literature (Simon, 2006), namely prediction, filtering and smoothing. A Kalman filter (KF) (Brown and Hwang, 1992) is the most commonly used algorithm for fusing the outputs of an integrated SINS/GPS system (Xu et al., 2010). It is well known that the precision of the optimal smoothing algorithm is theoretically higher than that of prediction and filtering, since the smoother can use more observations (Gelb, 1974). In general, most high-resolution earth observations deliver the imaging results after the missions are complete. Thus this paper considers the smoothing estimation algorithm for post processing. The Rauch-Tung-Striebel (R-T-S) smoother is a fixed interval smoother, consisting of a standard Kalman filter and a set of backward processing equations (Rauch et al., 1965; Lee and Jekeli, 2011). The smoothed state estimates are derived through propagating the scaled statistics of the forward filter backward in time (Durbin and Koopman, 2012). This smoothing method has already been used in the post data processing of a SINS/GPS integrated system (Kennedy et al., 2007).

However, to reduce the preparation time on the ground and enhance work efficiency, especially in more urgent situations (such as the survey of geological disaster, fire and flood), it is hoped that the SINS/GPS integrated system could be started up after the take-off and before the aircraft reaches the mission location. In this case, the uncertain errors of the initial attitude will be brought into the integrated SINS/GPS system. As misalignment of initial attitude error may now be very large, the linear SINS error model becomes inapplicable. Moreover, the performance of an R-T-S smoother based on a KF will degrade because of the neglected nonlinear error terms in the model. Therefore, a nonlinear smoothing algorithm should be considered.

The extended Kalman filter (EKF) based on linearizing the system model with a Taylor series expansion has been widely used in nonlinear systems (Haykin, 2001). However, the linearization will produce truncated errors and lead to poor performance and even divergence for a highly nonlinear system (Simon, 2006). The extended R-T-S smoother (ERTSS), which has a similar formulation to the R-T-S, is a corresponding nonlinear smoother based on EKF (Crassidis and Junkins, 2004; Sarkka et al., 2012). The sigma point Kalman filter (SPKF), a novel filter to overcome the shortcomings of EKF, has been proved to be far superior to EKF in a wide range of applications (Van der Merwe et al., 2004). It mainly comprises an unscented Kalman filter (UKF), central difference Kalman filter (CDKF), cubature Kalman filter among others (Julier et al., 1995; Ito and Xiong, 2000; Arasaratnam and Haykin, 2009; Wu, 2006). Sigma point filters have been used pervasively in the alignment of SINS and the data fusion of SINS/GPS systems (Crassidis, 2006; Wang et al., 2012;

Hao et al., 2010; Jwo and Lai, 2009). However, previous work mainly deals with real time processes and few discussions can be found on the subject of nonlinear smoothing problems. Based on Striling's interpolation formula, CDKF can capture the posterior mean and covariance accurately to 2nd-order (3nd-order is achieved for symmetric distribution) compared to EKF (Van der Merwe et al., 2004). The central difference R-T-S smoother (CDRTSS) was first proposed by Sarkka and Hartikainen (2010), which can give superior results for nonlinear systems by combining the CDKF and R-T-S smoother.

In this paper, we consider the implementation of the CDRTSS in integrated SINS/ GPS post-processing and apply it to airborne earth observation motion compensation. There is no need to align before take-off since CDRTSS possesses the ability to deal with large attitude errors. Simulation and flight tests are utilized to compare the performance of CDRTSS and ERTSS.

This paper is organized in six sections. The CDRTSS algorithm is presented in Section 2. Section 3 introduces the SINS error model based on an angle error model, and the implementation of CDRTSS in the integrated SINS/GPS system is described. In Section 4, numeric simulations and analyses are conducted through comparison between ERTSS and CDRTSS. Flight testing is conducted in Section 5 to analyse the performance of CDRTSS further and the paper is concluded in Section 6.

2. THE CDRTSS ALGORITHM. The ERTSS and CDRTSS possess the same form and are all derived from a R-T-S smoother. In the R-T-S smoother, the data is first processed by the forward filter, and then a backward recursion is used to compute the smoothing results based on the forward filtering outputs. The ERTSS has been discussed in several literatures and can be found in Simon (2006). In this section, a brief introduction of CDRTSS is presented.

Consider the following nonlinear system:

$$\begin{cases} x_k = f(x_{k-1}, k-1) + \Gamma_{k-1} w_{k-1} \\ z_k = h(x_k, k) + v_k \end{cases} \tag{1}$$

where x_k is the state vector and z_k is the measurement vector. $f(\cdot)$ is the dynamic model function and $h(\cdot)$ is the measurement model function. The process noise w_{k-1} and the measurement noise v_k are assumed to be Gaussian white noise with covariance Q_{k-1} and R_{k-1} respectively.

The forward process part of CDRTSS is a standard CDKF algorithm. Based on Stirling's interpolation formula, CDKF utilizes the prior distribution to create $2L+1$ (L is the state dimension) sigma points and then captures the posterior distribution by propagating the sigma-points through the dynamic and measurement models. The CDKF algorithm is given as follows (Ito and Xiong, 2000; Van der Merwe et al., 2004):

Initialization:

$$\hat{x} = E[x_0], \, P_{x_0} = E[(x_0 - \hat{x})(x_0 - \hat{x})^T] \tag{2}$$

(1) Calculate sigma-points for time-update

$$\hat{\chi}_{k-1} = [\, \hat{x}_{k-1} \quad \hat{x}_{k-1} + h\sqrt{P_{k-1}} \quad \hat{x}_{k-1} - h\sqrt{P_{k-1}} \,] \tag{3}$$

(2) Time-update equations

$$
\begin{cases}
\hat{\chi}_k^- = f(\hat{\chi}_{k-1}, k-1) \\
\hat{x}_k^- = \sum_{i=0}^{2L} w_i^m \hat{\chi}_{k,i}^- \\
P_k^- = \sum_{i=1}^{L} [w_i^{c1}(\hat{\chi}_{k,i}^- - \hat{\chi}_{k,L+i}^-)(\hat{\chi}_{k,i}^- - \hat{\chi}_{k,i+L}^-)^T \\
\quad + w_i^{c2}(\hat{\chi}_{k,i}^- + \hat{\chi}_{k,L+i}^- - 2\hat{\chi}_{k,0}^-)(\hat{\chi}_{k,i}^- + \hat{\chi}_{k,L+i}^- - 2\hat{\chi}_{k,0}^-)^T] + \Gamma_{k-1} Q \Gamma_{k-1}^T \\
C_k = \sqrt{P_{k-1}} \dfrac{1}{2h}(\hat{\chi}_{k,1:L}^- - \hat{\chi}_{k,L+1:2L}^-)^T
\end{cases}
\tag{4}
$$

(3) Calculate sigma points for measurement-update

$$
\hat{\chi}_k^{-*} = [\,\hat{x}_k^- \quad \hat{x}_k^- + h\sqrt{P_k^-} \quad \hat{x}_k^- - h\sqrt{P_k^-}\,]
\tag{5}
$$

(4) Measurement-update equations

$$
\begin{cases}
\hat{\Upsilon}_k^- = h(\hat{\chi}_k^{-*}, k); \\
\hat{y}_k^- = \sum_{i=0}^{2L} w_i^m \hat{\Upsilon}_{k,i}^-
\end{cases}
\tag{6}
$$

$$
\begin{cases}
P_{\tilde{y}_k} = \sum_{i=1}^{L} [w_i^{c1}(\hat{\Upsilon}_{k,i}^- - \hat{\Upsilon}_{k,L+i}^-)(\hat{\Upsilon}_{k,i}^- - \hat{\Upsilon}_{k,L+i}^-)^T \\
\quad + w_i^{c2}(\hat{\Upsilon}_{k,i}^- + \hat{\Upsilon}_{k,L+i}^- - 2\hat{\Upsilon}_{k,0}^-)(\hat{\Upsilon}_{k,i}^- + \hat{\Upsilon}_{k,L+i}^- - 2\hat{\Upsilon}_{k,0}^-)^T] + R \\
P_{x_k y_k} = \sqrt{w_i^{c1} P_k^-}[\hat{\Upsilon}_{k,1:L}^- - \hat{\Upsilon}_{k,L+1:2L}^-]^T
\end{cases}
\tag{7}
$$

$$
\begin{cases}
K_k = P_{x_k y_k} P_{\tilde{y}_k}^{-1} \\
\hat{x}_k = \hat{x}_k^- + K_k(y_k - \hat{y}_k^-) \\
P_k = P_k^- - K_k P_{\tilde{y}_k} K_k^T
\end{cases}
\tag{8}
$$

where the weights of each sigma-point are $w_0^m = (h^2 - L)/h^2$, $w_0^m = 1/(2h^2)$, $w_i^{c1} = 1/(4h^2)$, $w_i^{c2} = (h^2 - 1)/(4h^4)$. $h \geqslant 1$ is the scalar central difference interval size which determines the spread of the sigma points around the prior mean, and its optimal value is $\sqrt{3}$ for Gaussian distribution. The cross-covariance C_k between $\hat{x}_{k-1}$ and $\hat{x}_k^-$ is calculated for the backward process part.

During the processing of CDKF, the predicted state $\hat{x}_k^-$, estimated state $\hat{x}_k$, predicted covariance P_k^-, estimated covariance P_k and the cross-covariance C_k need to be stored at each filtering point for late backward recursion.

After the filtering estimates have been computed, the smoothed state estimation and its covariance can be computed using the following backward recursion (for $n = N - 1 \ldots 0$) (Sarkka and Hartikainen, 2010):

$$
\begin{cases}
K_k^S = C_{k+1}(P_{k+1}^-)^{-1} \\
\hat{x}_k^S = \hat{x}_k + K_k^S(\hat{x}_{k+1}^S - \hat{x}_{k+1}^-) \\
P_k^S = P_k + K_k^S(P_{k+1}^S - P_{k+1}^-)(K_k^S)
\end{cases}
\tag{9}
$$

Where the smoothing distribution and filtering distribution of the last time step N are the same, $\hat{x}_N^S = \hat{x}_N$ and $P_N^S = P_N$.

3. CDRTSS FOR THE SINS/GPS INTEGRATED SYSTEM.

3.1. *SINS error model*. The SINS error model, which is the foundation of the integrated SINS/GPS system, is established in this subsection. It includes the differential equation of attitude, velocity and position error (Goshen-Meskin and Bar-Itzhack, 1992). The coordinate frames used in this paper include the geocentric inertial frame (i-frame), earth-centered earth fixed frame (e-frame), navigation frame (n-frame), platform frame (p-frame) and body frame (b-frame). A detailed description of these coordinate frames is in Farrell and Barth (1998), and Crassidis (2006).

The differential equation of attitude error is given by (Groves, 2008):

$$\dot{\phi} = (I - C_n^p)\omega_{in}^n + \delta\omega_{in}^n - \hat{C}_b^n \varepsilon^b \tag{10}$$

where $\phi = [\, \phi_E \quad \phi_N \quad \phi_U \,]^T$ denotes the attitude error angle. The C_n^p is the direction cosine matrix (DCM) between the p-frame and the n-frame. ω_{in}^n is the rotation velocity vector of n-frame relative to i-frame expressed in n-frame, and $\delta\omega_{in}^n$ is the error of ω_{in}^n. C_b^n is the DCM between the n-frame and the b-frame, meanwhile $\hat{C}_b^n$ is the estimate of C_b^n. $\varepsilon^b = [\, \varepsilon_x \quad \varepsilon_y \quad \varepsilon_z \,]^T$ is the gyro drifts in the b-frame. $(I - C_n^p)\omega_{in}^n$ is the nonlinear term of attitude error equation.

The differential equation of the velocity can be described as follows:

$$\delta\dot{V} = (I - C_p^n)\hat{C}_b^n \hat{f}^b - (2\omega_{ie}^n + \omega_{en}^n) \times \delta V - (2\delta\omega_{ie}^n + \delta\omega_{en}^n) \times V + C_b^n \nabla^b \tag{11}$$

where $V = [\, V_E \quad V_N \quad V_U \,]^T$ is the velocity vector, and δV is the velocity error vector. $\hat{f}^b$ is the specific force measured by the accelerometers expressed in the b-frame. ω_{ie}^n is the rotation rate from the e-frame relative to the i-frame expressed in the n-frame and ω_{en}^n is the rotation rate from the n-frame relative to the e-frame expressed in the n-frame. $\delta\omega_{ie}^n$ and $\delta\omega_{en}^n$ are the error of ω_{ie}^n and ω_{en}^n, respectively. ∇^b is the bias of the accelerometer measurement expressed in the b-frame. $(I - C_p^n)\hat{C}_b^n \hat{f}^b$ is the nonlinear term of velocity error equation.

The differential equation of position error is given by:

$$
\begin{cases}
\delta\dot{L} = -\dfrac{V_N}{(R_M + h)^2}\delta h + \dfrac{1}{R_M + h}\delta V_N \\[2ex]
\delta\dot{\lambda} = -\dfrac{V_E \sin L}{(R_N + h)\cos^2 L}\delta L - \dfrac{V_E}{(R_N + h)^2 \cos L}\delta h + \dfrac{1}{(R_N + h)\cos L}\delta V_E \\[2ex]
\delta\dot{h} = \delta V_U
\end{cases} \tag{12}
$$

where $\delta L,\ \delta\lambda,\ \delta h$ are the errors of latitude, longitude and height, respectively. R_M and R_N are the main curvature radii along the meridian and the vertical plane of meridian, respectively.

3.2. *Design of the CDRTSS for integrated SINS/GPS system*. As we can see from Equations (10) and (11), the SINS error model is related to the gyro drift ε and the accelerometer bias ∇. To achieve better SINS error estimation accuracy, the gyroscope drift and accelerometer bias must be considered. The gyroscope drift and

accelerometer bias can be approximated as random noise, which includes a random constant process and a white Gaussian process. The constant drift and bias of the gyro and the accelerometer as well as the SINS errors are selected as the state vector. The random noise of the gyro and accelerometer are estimated as the model error. The state vector is as follows: $x = [\phi_E \quad \phi_N \quad \phi_U \quad \phi_E \quad \delta V_E \quad \delta V_N \quad \delta V_U \quad \delta L \quad \delta \lambda \quad \delta H \quad \varepsilon_x \quad \varepsilon_y \quad \varepsilon_z \quad \nabla_x \quad \nabla_y \quad \nabla_z]^T$. ε_x, ε_y, ε_z, ∇_x, ∇_y, ∇_z, are the constant drift and bias of the gyro and accelerometer in x, y and z directions respectively, which can be modelled by $\dot{\varepsilon} = 0$, $\dot{\nabla} = 0$. The continued system model of SINS/GPS is formed as $\dot{x}(t) = f(x, t) + Gw(t)$, where $w = [w_{\varepsilon_x} \quad w_{\varepsilon_y} \quad w_{\varepsilon_z} \quad w_{\nabla_x} \quad w_{\nabla_y} \quad w_{\nabla_z}]$ represents the gyro and accelerometer random noise with $E[ww^T] = Q$. Matrix G is given by:

$$G = \begin{bmatrix} \hat{C}_b^n & 0_{3\times3} \\ 0_{3\times3} & \hat{C}_b^n \\ 0_{9\times3} & 0_{9\times3} \end{bmatrix}$$

To transfer the continued model to discrete model, a four-step Runge-Kutta numerical solution is utilized in this paper. The observation vector is defined by $z = \begin{bmatrix} \delta V_E' & \delta V_N' & \delta V_U' & \delta L' & \delta \lambda' & \delta h' \end{bmatrix}^T$. $\delta V_E'$, $\delta V_N'$, $\delta V_U'$ represent the differences of the east velocity, north velocity and up velocity between the measurements of SINS and the GPS, respectively. δL, $\delta \lambda'$, $\delta h'$ represent the differences between the latitude, longitude, and height calculated from SINS and GPS outputs respectively. The observation noise $v = [v_{\delta V_E'} \quad v_{\delta V_N'} \quad v_{\delta V_U'} \quad v_{\delta L} \quad v_{\delta \lambda'} \quad v_{\delta h'}]^T$ represents GPS velocity and position measurement noises, and the observation matrix H is given by:

$$H = \begin{bmatrix} 0_{3\times3} & diag\{1, 1, 1\} & 0_{3\times3} & 0_{3\times6} \\ 0_{3\times3} & 0_{3\times3} & diag\{R_M + h, (R_N + h)\cos L, 1\} & 0_{3\times6} \end{bmatrix}$$

Since the measurement model is linear, the formulation of CDKF in Equations (5, 6, 7) can be simplified as follows:

$$\begin{cases} \hat{y}_k = H_k \hat{x}_k^- \\ P_{yy} = P_k^- H_k^T \\ P_{xy} = H_k P_k^- H_k^T + R_k \end{cases} \tag{13}$$

Figure 1 shows the computation procedure diagram of an integrated SINS/GPS system using CDRTSS.

In summary, the CDRTSS used for SINS/GPS integrated post-processing can be divided into two parts: the filter solution and the smoother solution. The relationship of these two parts based on the synthesis of numerical simulation results is shown in Figure 2. In the whole process of SINS/GPS integration, the filter and smoother are computed at the GPS sampling rate, and the strapdown navigator is computed at the SINS sampling rate. In general, the sampling rate of SINS is higher than that of GPS.

From Figure 2, it can be seen that the strapdown computing error grows with time during the interval of GPS data. Once the GPS data arrives, the slowly growing errors in the strapdown navigator can thus be limited by the feedback correction of filter and smoother. In the filtering solution, the V^F, P^F and A^F (denoting the velocity, position and attitude results of integration using filtering, respectively) would be corrected by using $\hat{x}_{f,k}$ (the state estimate of CDKF) at every filtering point. After the correction,
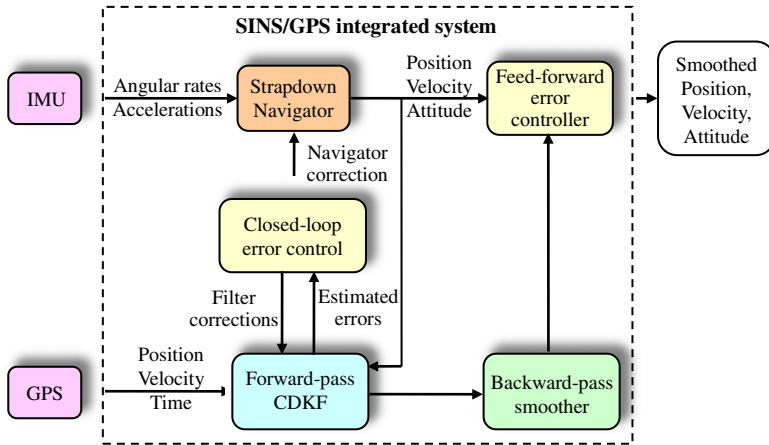
Figure 1. The computation procedure diagram of SINS/GPS integrated system using CDRTSS.
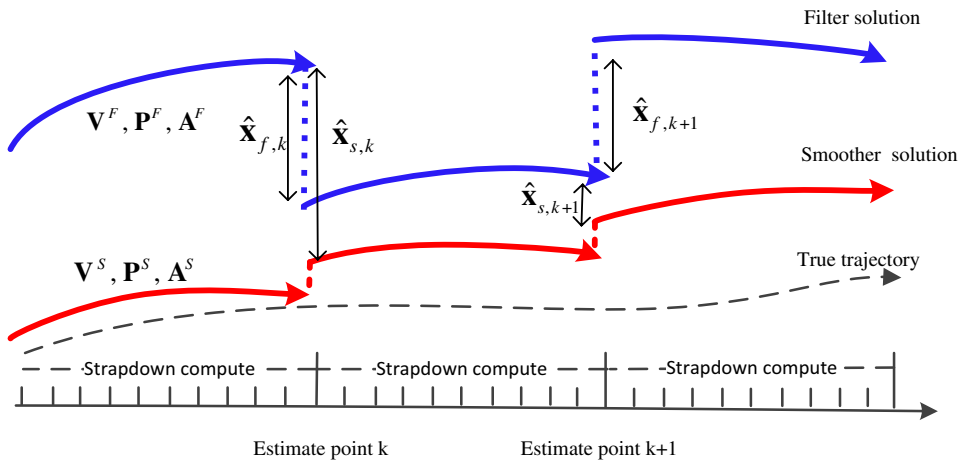

Figure 2. Relation between filter solution and smoother solution of CDRTSS.

$\hat{x}_{f,k}$ should be set to zero. In the smoothing solution, V^S, P^S and A^S (denoting the velocity, position and attitude results of integration using smoothing, respectively) should be corrected by using $\hat{x}_{s,k}$ (the state estimate of smoothing) at every smoothing point. The corrected velocity, position and attitude are regarded as the initial value of strapdown computation after every estimate point.

4. SIMULATION AND ANALYSIS.   To test and analyse the performance of CDRTSS, numerical simulations based on the simulated flight trajectory of an integrated SINS/GPS system have been conducted in this section.

   4.1. *Simulation design*.   In this subsection, a typical sequential U-form imaging flight trajectory with an S-manoeuvre at the beginning is used, as shown in Figure 3. The initial position is Latitude 40°N, Longitude 116°E and 500 m in height. The initial

Table 1. The mean STD of attitude error for 100 Monte-Carlo simulations (deg).

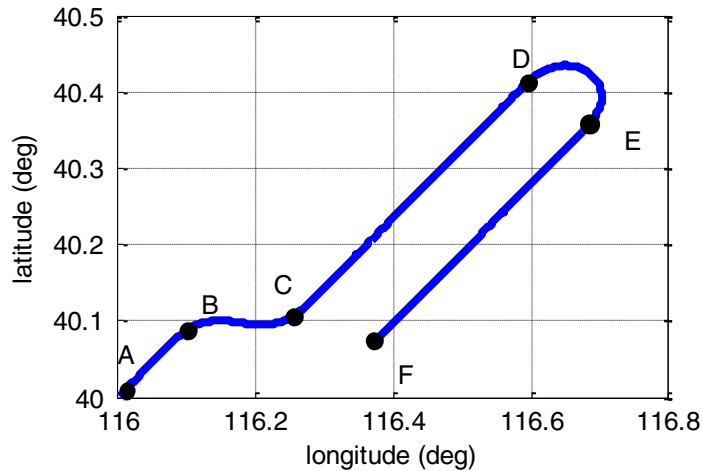| E[STD]	heading error	pitch error	roll error
ERTSS	0·06282	0·01576	0·01015
CDRTSS	0·03284	0·00952	0·00657

Figure 3. Trajectory of simulation.

heading is 040° and the velocity is 100 m/s during the flight. Firstly, the aircraft flies 100 s in a straight line, and after that there is an S-manoeuvre with 60° increase (100 s) and decrease (100 s) in heading direction. Then the aircraft flies 400 s straight before turning 180° clockwise in 200 s, and finally it flies 400 s straight again.

The errors of sensors in SINS/GPS integration are as follows: the gyro bias and white noise are all 0·2°/h, the accelerometer bias is 100 μg and the accelerometer white noise is 50 μg, the horizontal position noise is 0·1 m, the vertical position noise is 0·15 m, the horizontal velocity noise is 0·03 m/s, and the vertical velocity noise is 0·05 m/s. There is no outage in GPS data.

To test the performance of the CDRTSS and analyse the effect of different initial attitude errors on the precision of the integrated SINS/GPS estimation, three conditions with 10°, 20° and 30° initial attitude errors (the initial attitude includes heading, pitch, and roll) are designed, and the simulated data are processed by ERTSS and CDRTSS respectively.

4.2. *Simulation results and analysis.* The attitude estimate errors of CDRTSS and ERTSS in three conditions mentioned in Section 4.1 are shown in Figures 4, 5, 6. Moreover, the performance of CDRTSS and ERTSS with initial attitude error of 30° for a Monte-Carlo run of 100 randomly initialized experiments is summarized and compared in Table 1. Figure 4 illustrates that there is no distinct difference between the performance of the ERTSS and CDRTSS with 10° initial attitude error. Along with the initial attitude error increase, it is obvious that the CDRTSS gives better results than the ERTSS. Furthermore, the mean standard deviation (E[STD]) of
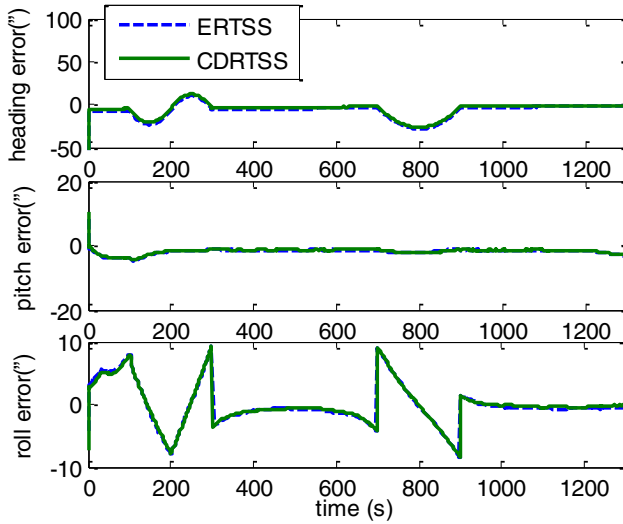
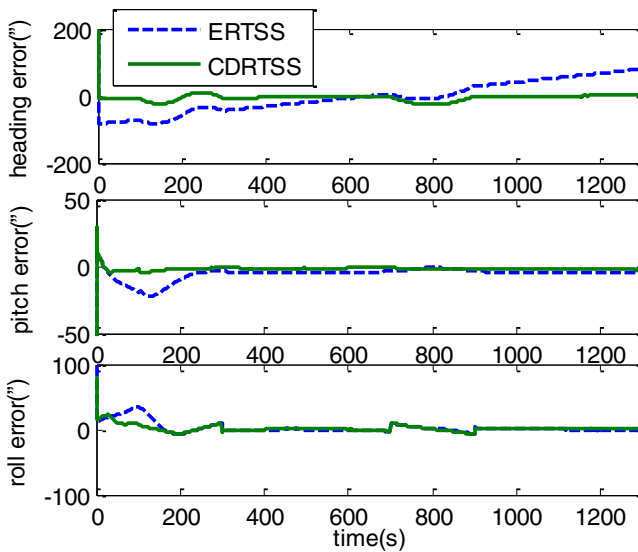Figure 4. Estimated attitude error with 10° initial attitude error.

Figure 5. Estimated attitude error with 20° initial attitude error.

attitude errors using the CDRTSS algorithm shown in Table 1 is much smaller than that of ERTSS, validating the superiority of the CDRTSS.

5. FLIGHT TEST AND DISCUSSION. The simulation tests, given in Section 4, have shown that the CDRTSS can obtain a better performance over ERTSS. How about the real application result of the CDRTSS? In this section, flight data will be used to validate the effectiveness of CDRTSS.
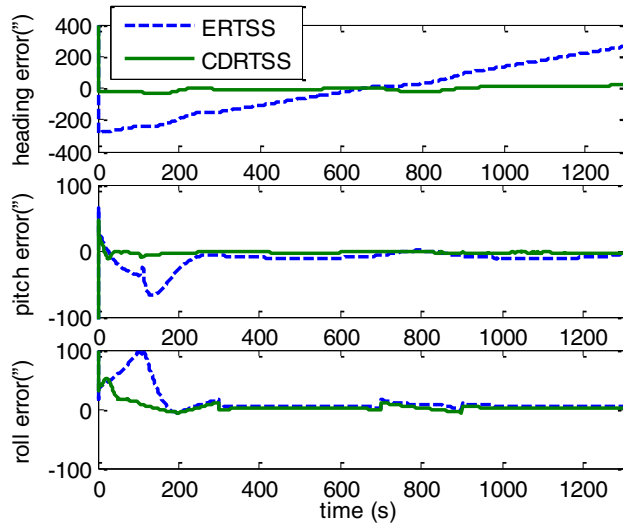
Figure 6. Estimated attitude error with 30° initial attitude error.
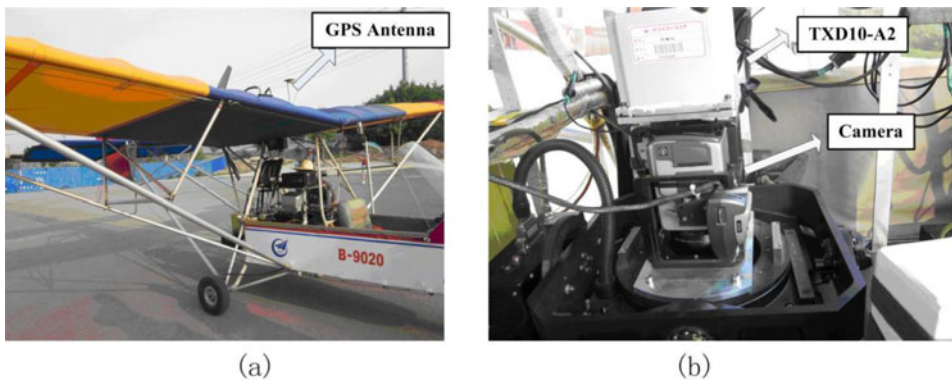
Figure 7. The test platform. (a) The A2C aircraft. (b) Sensor installation on the aircraft.

A two-hour flight test was carried out in a calibration field in Pingdingshan, China. This area has a large number of ground control points with their actual positions known in advance, which makes it possible to calculate the actual attitude and position of the aircraft through the photos it takes. The SINS/GPS integrated system is carried on an ultra-light A2C aircraft with the GPS antenna fixed on the top (seen in Figure 7(a)). The IMU (TXD10-A2) and the camera are placed in the cabin of the aircraft (see Figure 7(b)).

The integrated SINS/GPS system developed by Beihang University is used in the flight test, which consists of the Dynamically Tuned Gyroscope (DTG)-based IMU and the Trimble 5700 dual-frequency GPS receiver. The IMU comprises two HT-A3 dynamically tuned gyroscopes (HT-A3 precision strapdown flexible gyroscope, 1999) and three JHT-I-B quartz accelerometers (Jht-i-b quartz accelerometers, 1998). The sampling rates of the IMU and GPS are 100 Hz and 10 Hz respectively. The gyro
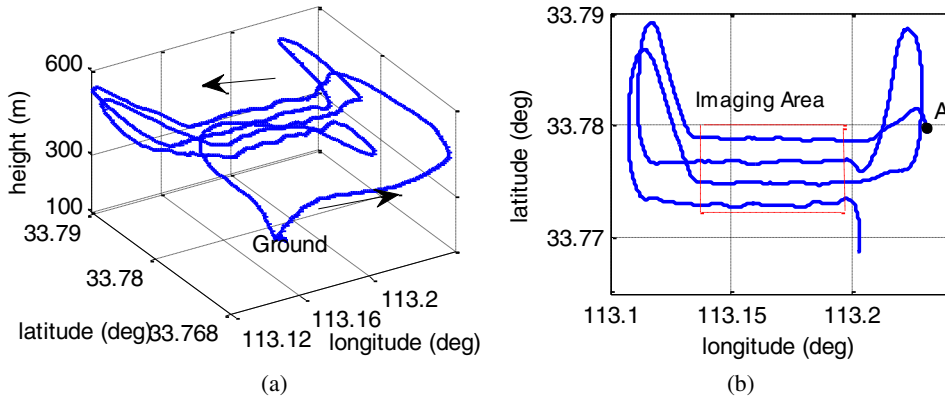
Figure 8. Flight trajectory. (a) three-dimensional trajectory. (b) two-dimensional trajectory.

constant and random drifts are 0·1°/h and the accelerometer constant and random biases are 100 μg. The post-processed position and velocity precision of GPS is 10 mm + 1·5 ppm and 0·01 m/s respectively. During the flight, the original output data of the integrated SINS/GPS system are stored by the PCS fixed in the cabin.

Figure 8(a) shows the trajectory of the flight measured by GPS. Point A in Figure 8 (b) can be seen as the time that the IMU started up and the imaging area is marked by the dashed line. There are four image segments, including about 2000s data. Each segment has a series of discrete image dots. Currently, the aero-triangulation method is recognized as a better way to calibrate the navigation data processed by SINS/GPS integration (Toth, 2002). In this flight test, the position and attitude information of higher precision are provided by Chinese Academy of Surveying and Mapping, which is computed by the aero-triangulation method with the well-signalized ground control points and the imaging data. This flight test was in good conditions with the sky very clear. This all ensures that aero-triangulation can obtain maximum positioning and attitude accuracy that can be used as the reference for SINS/GPS integration. In the in-flight startup case, the GPS can provide initial position and velocity information for the aircraft. In general, the approximate value of the initial heading can be acquired through the east and north velocity information from GPS. However, the accurate initial heading still remains unknown due to the existence of the drift angle induced by the wind speed and other factors. According to other flight tests, the drift angle is around 10° in fine weather and these values will increase in worse conditions. So we consider different cases with heading misalignment ranging from 5° to 30° increased by 5° steps. Moreover, there is no large pitch and roll during the preparation period, based on the many flight tests conducted. Hence, the maximal values of pitch and roll are both about 5° for this aircraft. Here, the pitch and roll can be initialized to zero and the misalignment is assumed to be 5°.

Figures 9 and 10 show the STD of latitude, longitude and altitude error with different initial heading errors using CDRTSS and ERTSS. From the figures, it can be seen that the estimated error of position using ERTSS climbs with the increase of initial heading error, whereas the performance of CDRTSS is very stable. Also, the precision of the positioning estimate of CDRTSS is better than that of ERTSS.
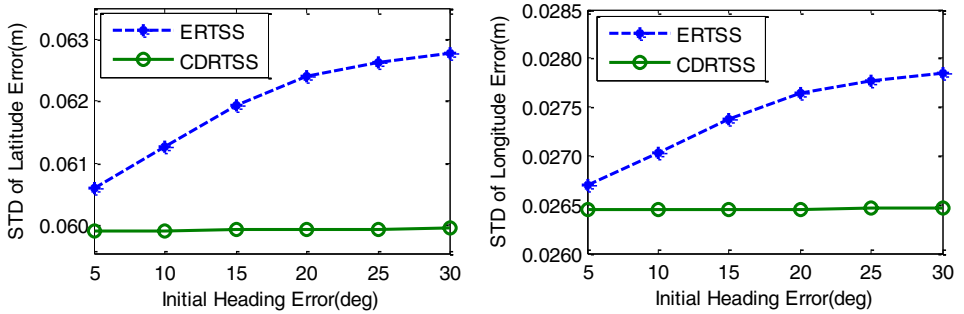
Figure 9. The STD of latitude and longitude error with different initial heading error.
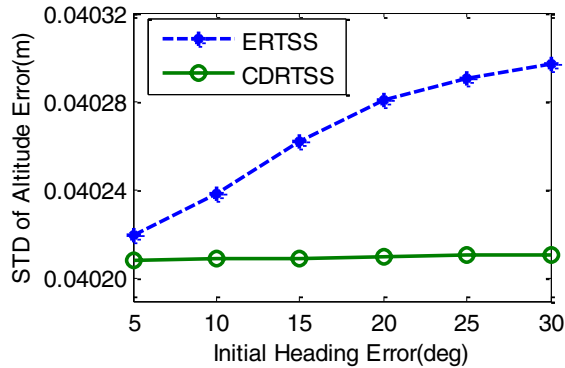

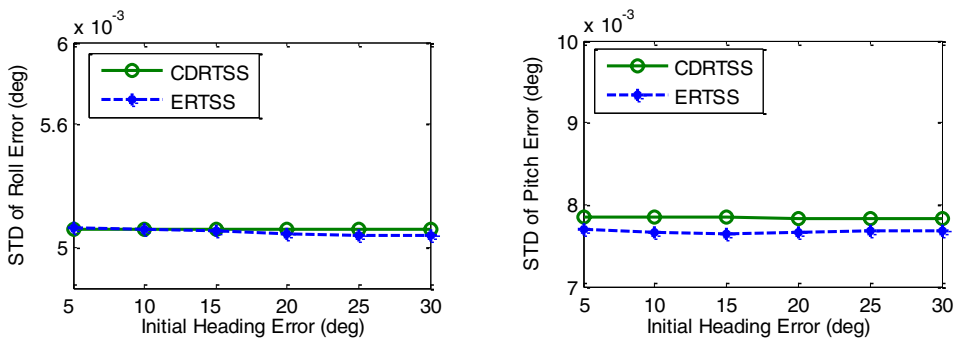Figure 10. The STD of altitude error with different initial heading error.

Figure 11. The STD of pitch and roll error with different initial heading error.

Figure 11 shows the STD of the pitch and roll error with different initial heading errors using CDRTSS and ERTSS. It can be seen that the STD of pitch and roll error using these two methods are very close and small due to high observability and the small initial horizontal misalignment error. The STD of the heading error shown in Figure 12 illustrates that the STD of heading error using CDRTSS is smaller and much more stable than that of ERTSS, which is further displayed in Table 2.

Table 2. STD of heading error in different cases (deg).

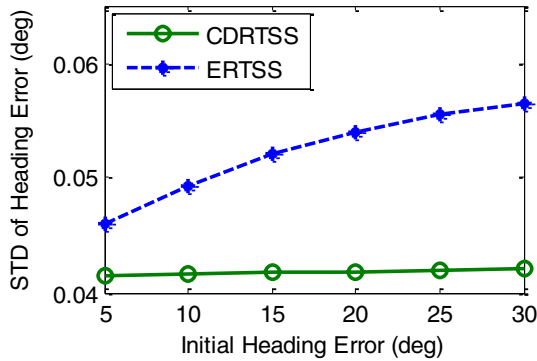| Initial heading error(deg)	5	10	15	20	25	30
ERTSS	0·0461	0·0492	0·0521	0·0540	0·0555	0·0565
CDRTSS	0·0415	0·0416	0·0418	0·0419	0·0420	0·0420

Figure 12. The STD of heading error with different initial heading error.
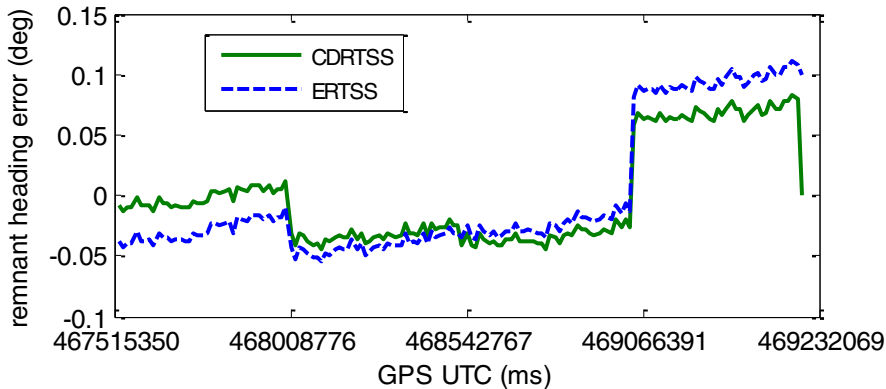

Figure 13. The remnant heading error with 30° initial heading error.

From the figures and tables above, it can be seen that the positioning precision of CDRTSS can be improved by several millimetres, while the heading precision can be improved by several percent of a degree. So, the remnant heading error (the absolute error subtracting the mean error) with 30° heading misalign is shown in Figure 13. It can be seen that the amplitude of CDRTSS is smaller than that of ERTSS and it is obvious that CDRTSS has great advantages over ERTSS. Undoubtedly, it is more effective.

6. CONCLUSION. In this paper, a nonlinear smoother algorithm called the Central Difference Rauch-Tung-Striebel (R-T-S) smoother (CDRTSS) based on a

Central Difference Kalman filter (CDKF) and Rauch-Tung-Striebel (R-T-S) smoother is presented and applied to the SINS/GPS integrated system post-processing under the in-flight startup condition. Compared with the commonly used Extended R-T-S Smoother (ERTSS), its performance has been analysed through numerical simulation and flight test. The results indicate that CDRTSS can obtain higher precision of positioning and attitude estimates than that of ERTSS. This provides a new estimation method for SINS/GPS integration used in airborne earth observation and other applications, including some emergency applications. However, this paper merely gives an evaluation of CDRTSS and ERTSS when GPS data is normal. GPS receivers sometimes do not function correctly due to signal blockage, attenuation and disturbance (which may lead to intermittent positions or unknown abnormal noise which are also known as outliers). How to ensure that a satisfactory navigation result can be obtained when there are outages or outliers in the GPS data is worthy of future research.

REFERENCES

Arasaratnam, I. and Haykin, S. (2009). Cubature Kalman filters. *IEEE Transactions on Automatic Control*, **54**(6), 1254–1269.

Brown, R.G. and Hwang, P.Y.C. (1992). *Introduction to random signals and Applied Kalman Filtering*. John Wiley and Sons. New York.

Crassidis, J.L. and Junkins, J.L. (2004). *Optimal Estimation of Dynamic Systems*. Chapman & Hall/CRC.

Crassidis, J.L. (2006). Sigma-point Kalman filtering for integrated GPS and inertial navigation. *IEEE Transactions on Aerospace and Electronic Systems*, **42**(2), 750–756.

Durbin, J. and Koopman, S.J. (2012). *Time series analysis by state space methods*, Oxford University Press.

Fang, J.C. and Gong, X.L. (2010). Predictive Iterated Kalman Filter for INS/GPS Integration and Its Application to SAR Motion Compensation. *IEEE Transactions on Instrumentation and Measurement*, **59** (4), 909–915.

Farrell, J. and Barth, M. (1998) *The Global Positioning System & Inertial Navigation*, New York: McGraw-Hill.

Gelb, A. (1974). *Applied Optimal Estimation*. The Analytic Science Corporation.

Goshen-Meskin, D. and Bar-Itzhack, I.Y. (1992). Unified Approach to Inertial Navigation System Error Modeling. *AIAA Journal of Guidance, Control and Dynamics*, **15**(3), 648–653.

Groves, P.D. (2008). *Principles of GNSS, inertial, and multisensor integrated navigation systems*, Artech House, London.

Hao, Y.L., Zhang, Z.Y. and Xia, Q.X. (2010). Research on Data Fusion for SINS/GPS Magnetometer Integrated Navigation based on Modified CDKF. *Conference on Progress in Informatics and Computing（PIC）*, 1215–1219.

HT-A3 precision strapdown flexible gyroscope (1999). Shaan Xi Spaceflight the Great Wall Technology Co. Ltd. http://www.ec21.com/product-details/HT-A3-Precision-Strapdown-Flexible-Gyroscope-4691830. html. Accessed 31 July 2013.

Haykin, S. (2001). *Kalman Filtering and Neural Networks*. John Wiley & Sons, Inc., New York.

Ito, K. and Xiong, K. (2000) Gaussian Filters for Nonlinear Filtering Problems. *IEEE Transactions on Automatic Control*, **45**(5), 910–927.

Jht-i-b Quartz Accelerometers (1998). Shaan Xi Spaceflight the Great Wall Technology Co.Ltd. http://www.ec21.com/product-details/Jht-i-b-Quartz-Accelerometers-4686310.html. Accessed 30 July 2013.

Jwo, D.J. and Lai, S.Y. (2009). Navigation integration using the fuzzy strong tracking unscented Kalman Filter. *The Journal of Navigation*, **62**, 303–322.

Julier, S.J., Uhlmann, J.K. and Durrant-Whyte, H.F. (1995). A new approach for filtering nonlinear systems. *Proceedings of the 1995 American Control Conference*, 1628–1632.

Kennedy, S., Cosandier, D. and Hamilton, J. (2007). GPS/INS Integration in Real-Time and Post-processing with NovAtel's SPAN System. *International Global Navigation Satellite Systems Society Symposium 2007*, Sydney.

Kim, T.J. (2004). Motion Measurement for High-Accuracy Real-Time Airborne SAR. *Proceedings of SPIE-The International Society for Optical Engineering, Radar Sensor Technology VIII and Passive Millimeter-Wave Imaging Technology* VII, 5410, 36–44.

Lee, J.K. and Jekeli, C. (2011). Rao-Blackwellized Unscented Particle Filter for a Handheld Unexploded Ordnance Geolocation System using IMU/GPS. *The Journal of Navigation*, **64**, 327–340.

Rauch, H., Tung, F. and Striebel, C. (1965). Maximum likelihood estimates of linear dynamic systems. *AIAA Journal*, **3**(8), 1445–1450.

Sarkka, S. and Hartikainen, J. (2010). Sigma point methods in optimal smoothing of non-linear stochastic state space models. *IEEE International Workshop on Machine Learning for Signal Processing (MLSP)*, 184–189.

Sarkka, S., Viikari, V., Huusko, M. and Jaakkola, K. (2012). Phase-Based UHF RFID Tracking with Non-Linear Kalman Filtering and Smoothing. *IEEE Sensors Journal*, **12**(5), 904–910.

Simon, D. (2006). *Optimal State Estimation: Kalman, H-Infinity, and Nonlinear Approaches*. Wiley & Sons. First edition.

Toth, C.K. (2002). Sensor integration in airborne mapping. *IEEE Transactions on Instrumentation and Measurement*, **1**(6), 1367–1373.

Van der Merwe, R., Wan, E.A., and Julier, S. (2004). Sigma-Point Kalman Filters for Nonlinear Estimation and Sensor-Fusion: Applications to Integrated Navigation. *Proceedings of the AIAA Guidance, Navigation & Control Conference (GNC)*, Providence, Rhode Island, 1735–1764.

Wang, Y.F., Sun, F.C., Zhang, Y.A. and Min, H.B. (2012). Central Difference Particle Filter Applied to Transfer Alignment for SINS on Missiles. *IEEE Transactions on Aerospace and Electronic Systems*, **48**(1), 375–387.

Wu, Y., Hu, D., Wu, M., and Hu, X. (2006). A numerical integration perspective on Gaussian filters. *IEEE Transactions on Signal Processing*, **54**(8), 2910–2921.

Xu, Z., Li, Y., Rizos, C. and Xu, X. (2010). Novel hybrid of LS-SVM and Kalman filter for GPS/INS integration. *The Journal of Navigation*, **63**, 289–299.